coatings

MDPI

Article

Effect of Si_3N_4/TaC Particles on the Structure and Properties of Microarc Oxidation Coatings on TC4 Alloy

Wei Gao [1], Liqun Wang [2], Yaohua Jin [1], Yuhong Yao [1], Zhisong Ding [1], Wei Yang [1,*] and Jiangnan Liu [1,*]

[1] School of Materials Science and Chemical Engineering, Xi'an Technological University, Xi'an 710032, China
[2] School of Physics, Xi'an Jiaotong University, Xi'an 710049, China
* Correspondence: yangwei_smx@163.com (W.Y.); liujiangnan@xpu.edu.cn (J.L.);
Tel.: +86-029-8617-3369 (W.Y.); +86-029-8617-3324 (J.L.)

Abstract: Si_3N_4/TaC composite MAO coatings were fabricated by microarc oxidation (MAO) on a Ti–6Al–4V (TC4) alloy in a phosphate-based electrolyte containing Si_3N_4/TaC mixed particles. The influence of the amount of Si_3N_4/TaC particles on the microstructure, composition, tribological behavior, and corrosion properties of the MAO coatings has been investigated. Morphological research of the MAO coatings was carried out using scanning electron microscopy (SEM), with the surface porosity analyzed by ImageJ software. X-ray diffraction (XRD) was used for the detection of the phase characteristic of the MAO coatings, and an abrasive wear test and electrochemical measurements were conducted in the artificial seawater solution by the ball-on-disc friction tester and the electrochemical workstation, respectively. The results showed that Si_3N_4/TaC particles could be successfully incorporated into the composite coatings, and the addition of Si_3N_4/TaC particles greatly reduced the porosity of the coatings, thus improving both tribological and corrosion properties of the composite MAO coatings. The composite MAO coating with the addition of 1 g/L Si_3N_4 + 0.5 g/L TaC particles showed the best tribological property and the optimum corrosion properties.

Keywords: microarc oxidation; TC4 alloy; Si_3N_4/TaC particles; porosity; tribological property; electrochemical corrosion

check for updates

Citation: Gao, W.; Wang, L.; Jin, Y.; Yao, Y.; Ding, Z.; Yang, W.; Liu, J. Effect of Si_3N_4/TaC Particles on the Structure and Properties of Microarc Oxidation Coatings on TC4 Alloy. *Coatings* **2022**, *12*, 1247. https://doi.org/10.3390/coatings12091247

Academic Editor: Francesco Marra

Received: 23 July 2022
Accepted: 23 August 2022
Published: 26 August 2022

1. Introduction

Titanium alloys are widely used in aerospace, marine, and biomedical fields due to their low density, high specific strength, low thermal expansion coefficient, and excellent biocompatibility [1–4]. However, their low hardness, poor tribological properties, and high electrode potential give rise to the problems such as surface abrasion, contact corrosion, and marine biofouling, thus limiting the extensive applications in the complicated marine environment [5]. At present, some surface modification methods, such as anodizing [6,7], vapor deposition [8], magnetron sputtering [9], microarc oxidation (MAO) [10,11], etc., [12–15] are used to improve the corrosion resistance and wear resistance of the aluminum, magnesium, and titanium alloys. Moreover, as an in situ growth technique for preparing ceramic coatings, MAO has some attractive characteristics such as easy operation, high production efficiency, and environmental friendliness, thus being widely used in the surface modification of titanium alloys [16]. It is well known that the high temperature and high pressure used in the process of MAO lead to coatings that contain a high density of pores. Thus, many studies have focused on improving the microstructures and properties of the coatings via optimizing the electrical conditions, such as the applied voltage/current magnitude, mode, frequency, and duty cycle via modifying the electrolyte compositions [16–23]. Recently, some functional particles such as Al_2O_3, ZrO_2, CeO_2, MoS_2, etc. [24–30], have been successfully introduced to the electrolyte to enhance the functional properties of titanium alloys. Wang et al. [27] confirmed that the composite ceramic coating containing Al_2O_3 on a Ti–6Al–4V (TC4) alloy exhibited better wear resistance at 300 °C due to the dense surface structure and higher volume fraction of Al_2TiO_5. Mu et al. [28] added

MoS_2 to the electrolyte to greatly reduce the friction coefficient of the MAO coatings on TC4 alloy. Chen et al. [29] also introduced MoS_2 particles into the electrolyte and proved that MoS_2 was able to retard the formation of micropores during the processing of MAO and thus significantly improving the corrosion resistance of the MAO coating, which would expand the application of TC4 alloy in the marine environment. Ao et al. [30] fabricated the TiO_2/hBN composite coating on the surface of Ti–6Al–4V alloy via microarc oxidation and found that the composite coating consisting of rutile TiO_2, anatase TiO_2, and an hBN phase was less porous than the particle-free coating and that the presence of hBN particles in the MAO coating could improve its anti-friction property.

Silicon nitride (Si_3N_4) ceramics that have a low thermal expansion coefficient, good mechanical properties at high temperatures, high thermal shock resistance and high resistance to chemical attack, and good tribological properties are widely used in manufacturing the Si_3N_4-based composite used in high-temperature applications. Some works have been conducted to prepare Si_3N_4 composite MAO coatings on magnesium alloys, pure Ti, and TC4 alloy [31–34]. Lou et al. [31] revealed that the addition of 2 g/L Si_3N_4 to the electrolyte made the MAO coatings on AZ31 Mg alloy have optimal corrosion resistance, a low friction coefficient, and good adhesion strength. However, Lu et al. [32] found that Si_3N_4 particles were difficult to incorporate into the coating due to their high melting point and that large Si_3N_4 particles had a negative effect on the coating thickness. As a result, the addition of Si_3N_4 particles did not enhance the corrosion resistance [32]. Aliofkhazraei et al. [33] successfully fabricated Si_3N_4/TiO_2 nanocomposite coatings by MAO on commercially pure titanium samples in a suspension with fine Si_3N_4 nanoparticles and found the coatings have high hardness and good wear resistance. In addition, our previous work [34] also demonstrated that the Si_3N_4 composite MAO coatings on a TC4 alloy fabricated by the addition of 1 g/L and 3 g/L Si_3N_4 had the best antibacterial property and wear resistance, respectively.

Tantalum carbide (TaC) is one of the common metal carbides with excellent physical and chemical properties such as high hardness (20 GPa), high melting point (3880 °C), excellent wear resistance, chemical stability, and so on [35]. Ding et al. [36] successfully prepared the TaC composite coatings by MAO on TC4 alloy and found that the coatings, when prepared with the addition of 5 g/L TaC, had the best wear resistance and corrosion resistance in seawater.

Based on previous research [34,36], the present study aims to take full advantage of the high hardness and excellent wear resistance of both TaC and Si_3N_4 particles as well as the good lubrication of Si_3N_4 particles to prepare the Si_3N_4/TaC composite MAO coatings on the surface of the TC4 alloy. Therefore, Si_3N_4 and TaC mixed particles were introduced into the phosphate-based electrolyte. The microstructure, wear resistance, and corrosion properties of the Si_3N_4/TaC composite MAO coatings were investigated to provide technical support for the applications of titanium alloy in marine environments.

2. Materials and Methods

2.1. Materials

Ti–6Al–4V alloy with 6.6% Al, 4.3% V, 0.1% Fe, and balance Ti (in wt. %) was used as the substrate material. The plate specimens, with the dimensions of φ20 mm × 5 mm, were sequentially ground with alumina waterproof abrasive paper up to 1200 grit and ultrasonically degreased in acetone for 10 min, followed by rinsing with distilled water and then dried in warm air.

2.2. MAO Treatment

MAO is a plasma-chemical and electrochemical process that combines electrochemical oxidation with a high voltage spark treatment in an aqueous electrolyte, leading to the formation of a physically protective oxide film or a ceramic-like coating on the metal surface to improve wear and corrosion resistance. The specimens were treated using the microarc oxidation equipment (JHMAO–60, XAUT, Xi'an, China) with a pulse power un-

der the following conditions: a constant voltage of 450 V, a frequency of 750 Hz, and a duty cycle of 3% for 10 min in the base electrolyte solution containing 20.0 g/L $(NaPO_3)_6$, 3.0 g/L Na_2WO_4, 3.0 g/L KF, 3.0 g/L KOH, and 5.0 g/L $CuSO_4$. For the lower porosity of the MAO coating with the addition of 4 g/L Si_3N_4 or 2 g/L TaC to the electrolyte solution obtained in the preliminary experimental results, a certain proportional concentration of Si_3N_4 nanoparticles (about 50 nm) and TaC microparticles (1–2 μm), i.e., 1 g/L Si_3N_4 + 0.5 g/L TaC, 2 g/L Si_3N_4 + 1 g/L TaC, 4 g/L Si_3N_4 + 2 g/L TaC, were added into the base electrolyte. The coated specimens prepared with the addition of 0 g/L, 1 g/L Si_3N_4 + 0.5 g/L TaC, 2 g/L Si_3N_4 + 1 g/L TaC, 4 g/L Si_3N_4 + 2 g/L TaC are simplistically denoted as 0 g/L, 1 g/L + 0.5 g/L 2 g/L + 1 g/L, and 4 g/L + 2 g/L Ta, respectively. The MAO process of the TC4 alloy is shown schematically in Figure 1, where the TC4 substrate was connected to the anode, and a 316 L stainless steel container was connected to the cathode. During the MAO process, the stainless steel barrel was put into the circulation cooling water tank to maintain the temperature of the electrolyte solution below 30 °C. The electrolyte was continuously stirred by both an electric stirrer with a speed of 300 r/min and an air stirrer with a displacement of 10 L/min to maintain the uniform distribution of the particles in the electrolyte. After the MAO process, the samples were rinsed in distilled water and then dried in warm air.

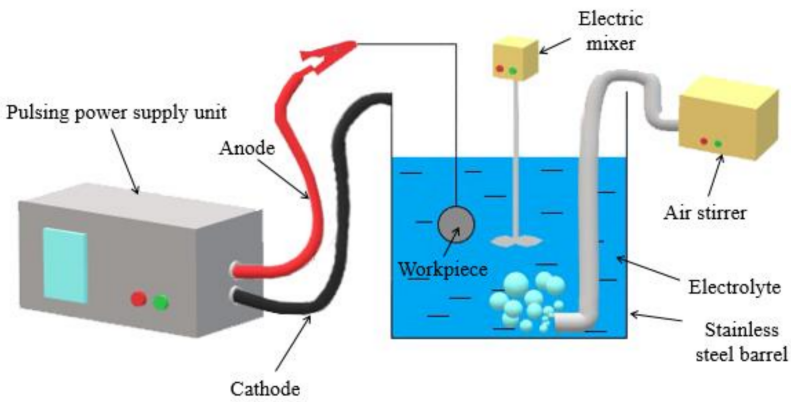

Figure 1. Schematic diagram of MAO process for TC4 alloy.

2.3. Surface Morphologies

The surface morphologies and element distribution of the MAO coatings were characterized by a scanning electron microscope (SEM, VEGA3–SBH, TESCAN, Brno, Czech Republic) operating in the secondary electron mode with an accelerating voltage of 30 kV and Oxford Inca X–Max energy dispersive spectrometry (EDS, Oxford Instruments plc, Oxford, UK), respectively. The surface porosity and the number of both the microholes and Si_3N_4 or TaC particles in the MAO coatings were quantified using ImageJ v1.48u software (NIH, Bethesda, Rockville, MD, USA, version 1,48u). Moreover, the thickness of the MAO coatings was measured using a TT260 eddy current thickness meter (Beijing TIME, Beijing, China) with an accuracy of 0.1 μm. Six measurements were conducted for each sample.

2.4. Phase Composition

The phase constituents of the coatings were detected at room temperature by an X-ray diffractometer (XRD, Bruker D8 DISCOVER A25, Bruker, Billerica, MA, USA) with Cu K_α (λ = 0.15405 nm) radiation at 30 kV and 40 mA. The XRD patterns were obtained in the 2θ ranging from 20° to 100° at a scanning speed of 2°/min.

2.5. Electrochemical Research

The corrosion properties of the coatings were evaluated by the electrochemical workstation (CHI 660C) attached to a typical three-electrode cell setup consisting of a specimen as the working electrode and a saturated calomel as the reference electrode (SCE), and a platinum sheet as the counter electrode. The electrochemical polarization measurements were carried out with a scan rate of 5 mV/s in the artificial seawater solution (Table 1). Before every measurement, the artificial seawater solution was deaerated by bubbling purified nitrogen gas for 1 h to eliminate the effect of the dissolved oxygen, and then the open current potential (OCP) was firstly recorded for 15 min to yield a state potential. The potentiodynamic polarization curves were plotted after the specimen was corroded freely for about 30 min to reach a quasi-stationary value of OCP. The corrosion potential (E_{corr}) and the corrosion current density (I_{corr}) of both TC4 alloy and the MAO coatings were calculated by fitting Tafel polarization curves with corrView software (version 3.1.0).

Table 1. Composition of the artificial seawater solution.

Chemical Reagents	Concentration, g/L
NaCl	24.53
$MgCl_2 \cdot 6H_2O$	11.11
Na_2SO_4	4.09
$CaCl_2$	1.16
KCl	0.70
$NaHCO_3$	0.20
KBr	0.10

2.6. Friction Tests

The tribological performance of both the TC4 alloy and the MAO coatings was evaluated at room temperature in the artificial seawater solution (Table 1) using a ball-on-disc friction tester (HT–1000 TRIBOLAB, ZKKH Co., Ltd., Lanzhou, China). The coatings or TC4 alloy served as the discs, and a GCr15 steel ball with a diameter of 5 mm served as the loading medium. A 5 N load was applied downward through the steel ball against the TC4 substrate and the MAO coatings at a constant sliding rate of 0.1 m/s. Each wear test lasted for 30 min. After the friction test, the morphologies and element distribution of the wear scars were also observed by SEM with Oxford Inca X–Max energy dispersive spectrometry (Oxford Instruments plc, Oxford, UK).

3. Results

3.1. Composition and Microstructure

The surface morphologies of both the ground TC4 and the MAO coatings with different concentrations of Si_3N_4/TaC particles are shown in Figure 2. As shown in Figure 2, there were some scratches and small pores of 1–2 μm on the surface of the ground TC4 alloy (Figure 2a); regardless of the Si_3N_4/TaC particles, there were many crater-like holes of different sizes in the coatings formed by the spark discharge and gas bubbles throughout the discharge channels during the MAO process, where the melted materials were expelled by the discharge and could not flow back to fill the discharge channels before their solidification [37,38]. Moreover, some significant changes could also be observed on the surface of the MAO coatings with the addition of the Si_3N_4/TaC particles (Figure 2c–e). For example, there were some microcracks in the MAO coatings with the Si_3N_4/TaC particles, which may be attributed to the fact that the particle additions block the flow of the melted metal, thus leading to the formation of the microcracks. On the other hand, it was found that some bright particles adhered to the surfaces of the coatings and that both the number and the size of the bright particles increased with the increasing Si_3N_4/TaC particle concentration (Figure 2c–e), indicating that the Si_3N_4 or TaC particles might be involved in the reaction of the MAO process. To further reveal the effect of the addition of the Si_3N_4/TaC particles on the MAO coatings, the number density and the size of microholes, the number

density of the bright particles, and the thickness of the MAO coatings were quantified. The results are given in Figure 3 and Table 2, showing that the thickness of the composite MAO coatings gradually increased with the increment of the concentration of Si_3N_4/TaC particles (Figure 3), which probably resulted from the inert or partly reactive incorporation of Si_3N_4/TaC particles into the oxide layer [21,27,29,30]. Compared with the MAO coating without Si_3N_4/TaC particles, the addition of Si_3N_4/TaC particles made the porosity significantly decrease. However, further increasing the concentration of Si_3N_4/TaC particles gave rise to a slight increment in the porosity (Figure 3). The previous studies also reported that the addition of the ceramic particles to the electrolyte reduced the porosity and average size of the micropores in the MAO coatings [25,27,30–33]. With increasing the concentration of Si_3N_4/TaC particles, the microarc discharge was more intense and allowed the particles to sinter together, which was evident by the observation of the larger bright particles in the coating with a higher concentration of Si_3N_4/TaC particles (Figure 2e). Meanwhile, a high concentration of Si_3N_4/TaC particles caused the ability of the particles to fill the microholes weaken during the MAO process and thus a slightly higher porosity, number density, and average size of the microholes were observed in the MAO coating with a high concentration of Si_3N_4/TaC particles. This well explained why the coatings with 1 g/L Si_3N_4 + 0.5 g/L TaC particles had the relevantly flat surface with the lowest porosity, the smallest average size, and number density of the microholes. Ding et al. [36] reported that the addition of TaC particles was beneficial to fill the micropores formed by the spark discharge during MAO process to make the surface become flat. Similar results were also reported in the MAO coatings incorporated by some hard particles (Cr_2O_3, Al_2O_3, etc.) [26,27,39].

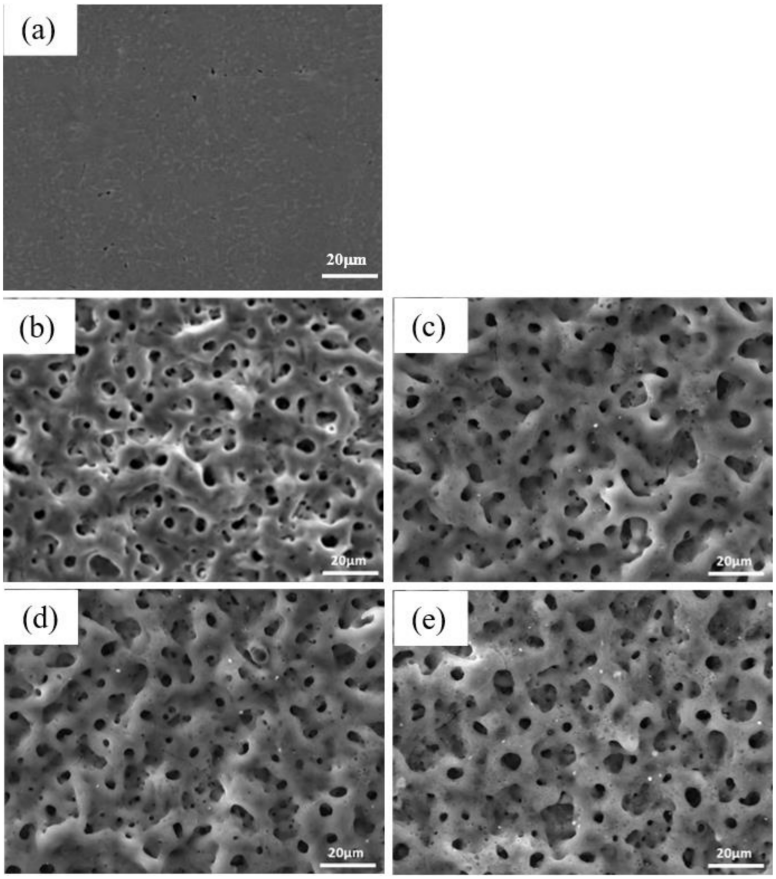

Figure 2. Surface morphologies of the ground TC4 alloy and the MAO coatings with different concentration of Si_3N_4/TaC particles: (**a**) TC4; (**b**) 0 g/L; (**c**) 1 g/L Si_3N_4 + 0.5 g/L TaC; (**d**) 2 g/L Si_3N_4 + 1 g/L TaC; (**e**) 4 g/L Si_3N_4 + 2 g/L TaC.

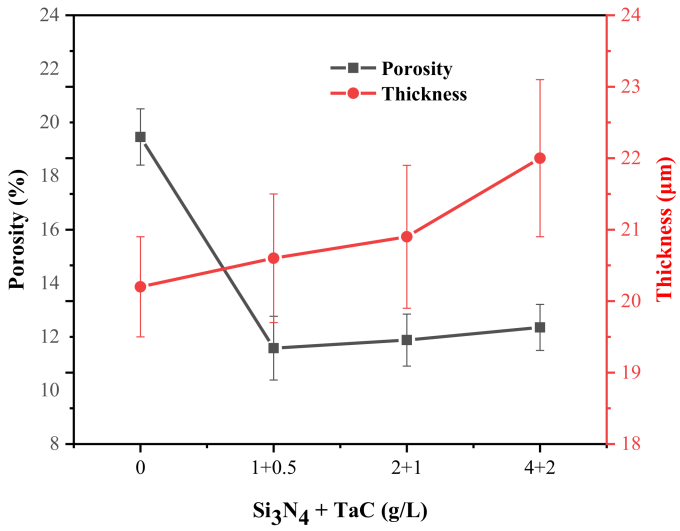

Figure 3. Surface porosity and thickness of the composite MAO coating with different concentration of Si_3N_4/TaC particles.

Table 2. Surface characteristic of the MAO coatings with different concentration of Si_3N_4/TaC particles.

Specimen	Surface Density of the Microholes, Number/mm^2	Average Diameter of the Microholes, μm	Surface Density of the Bright Particles, Number/mm^2
0 g/L	25,316 ± 1751	1.835 ± 1.275	0
1 g/L + 0.5 g/L	16,652 ± 1335	1.740 ± 1.226	2005 ± 151
2 g/L + 1 g/L	17,426 ± 1811	1.771 ± 0.861	3828 ± 202
4 g/L + 2 g/L	17,543 ± 2002	1.794 ± 1.136	5845 ± 346

The EDS mappings of the MAO coatings in Figure 4, especially in the enlarged image in Figure 4d, confirm that the bright particles were enriched with Ta and Si, which supported the incorporation of some Si_3N_4/TaC particles in the composite coatings that caused the number of the holes to decrease and the surface flatten. Table 3 shows the average compositions of the surfaces of the MAO coatings with different concentrations of Si_3N_4/TaC particles. Table 4 presents the EDS results of regions A (bright particle 1), B (bright particle 2), and C in the MAO coatings with the addition of 4 g/L Si_3N_4 + 2 g/L TaC particles, showing that some bright particles were enriched in Si, while others were enriched in Ta. As the plasma temperature during the MAO process was lower than the melt temperature of Si_3N_4 (1900 °C) and TaC (3880 °C), Si_3N_4 or TaC particles might be inertly absorbed onto or sintered to the MAO coatings. However, the size of the Si-rich particle in region A in Figure 4d was about 800 nm, which was much larger than the average size of the Si_3N_4 particles (about 50 nm). This suggested that the Si_3N_4 particles were very likely melted during the MAO process. In fact, it was reported that the melting point of the nano-sized particles decreased with the decreasing particle size [40,41]. It was likely that the nano-sized Si_3N_4 particles were reactively incorporated into the MAO coatings.

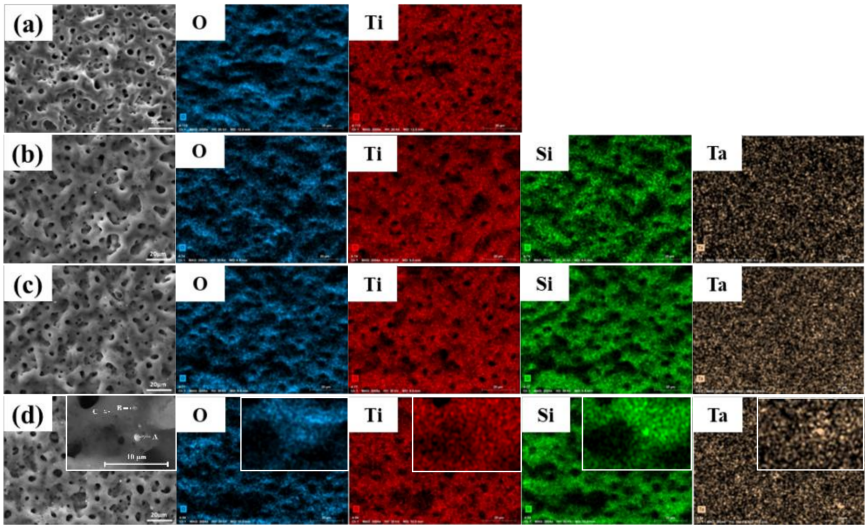

Figure 4. EDS mappings of the MAO coatings with different concentration of Si_3N_4/TaC particles: (**a**) 0 g/L; (**b**) 1 g/L Si_3N_4 + 0.5 g/L TaC; (**c**) 2 g/L Si_3N_4 + 1 g/L TaC; (**d**) 4 g/L Si_3N_4 + 2 g/L TaC.

Table 3. Percentage of elements in the MAO coatings with different concentration of Si_3N_4/TaC particles (at. %).

Specimen	O	Ti	Si	Ta
0 g/L	69.3	20.5	-	-
1 g/L + 0.5 g/L	68.5	19.6	3.2	0.2
2 g/L + 1 g/L	67.5	19.0	5.6	0.6
4 g/L + 2 g/L	66.8	15.8	11.6	1.0

Table 4. EDS results of region A, B, and C in the enlarged image in Figure 4d (at. %).

Region	O	Ti	Si	Ta
A	42.0	23.4	25.3	3.5
B	60.1	13.5	11.0	8.5
C	55.5	20.2	17.0	1.0

The phase constituents of the MAO coatings with different contents of Si_3N_4/TaC particles were investigated by XRD. The results are illustrated in Figure 5, and they show that the MAO coatings formed in the absence of Si_3N_4/TaC particles were mainly composed of anatase-type TiO_2 and rutile-type TiO_2, while both the TaC phase and Si_3N_4 phases could be detected in the coatings with the addition of the Si_3N_4/TaC particles. Moreover, by increasing the concentration of Si_3N_4/TaC particles, the peak intensity of rutile TiO_2 and TaC gradually increased, which was confirmed by the SEM results, i.e., the amounts of the Si-rich or Ta-rich bright particles increased with the increasing concentration of the Si_3N_4/TaC particles (Figure 2c–e). The formation of $Al_4Ti_2SiO_{12}$ may be associated with high temperature and high pressure during the MAO process. Wang et al. [27] found that Al_2TiO_5 in the Si_3N_4/Al_2O_3 composite coatings formed on TC4 alloy by MAO in the electrolyte with Al_2O_3 particles. The occurrence of $Al_4Ti_2SiO_{12}$ and the decrease in the metastable anatase-TiO_2 suggested that Al_2TiO_5 might react with Si_3N_4 to form $Al_4Ti_2SiO_{12}$ during localized high temperature and high pressure in the process of MAO. Aliofkhazraei et al. [33] fabricated Si_3N_4/TiO_2 nanocomposite coatings on commercially pure Ti and found the existence of $Si_4Al_2O_2N_6$ in the composite coatings.

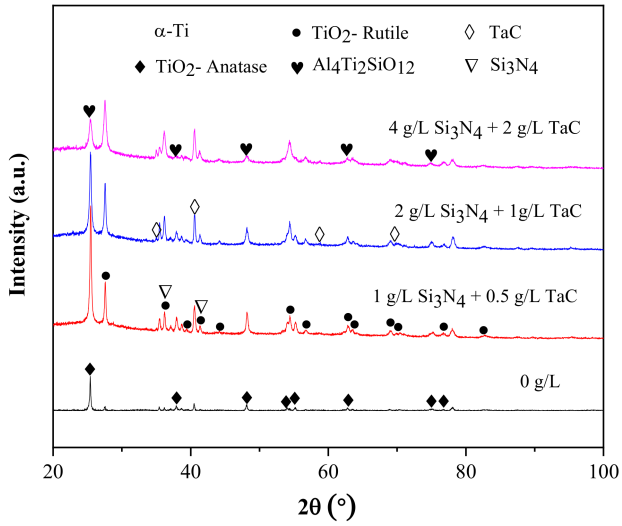

Figure 5. XRD patterns of the MAO coatings with different concentration of Si_3N_4/TaC particles.

This indicated that the Si_3N_4 particles were partially reactively incorporated into the composite MAO coatings, which was inconsistent with the results from Lu et al. [32]. Figure 3 shows that with an increasing Si_3N_4/TaC concentration, the thickness of the coatings increased slightly from 20.2 μm for the coating without Si_3N_4/TaC particles to 22.0 μm for the coating with the addition of 4 g/L Si_3N_4 + 2 g/L TaC particles, which contributed to the incorporation of the Si_3N_4 and TaC particles into the composite coatings during the process of MAO. Similar results were also reported in some studies [26,27,30], i.e., the excessive addition of the particles produced a large number of particles in the composite coatings and a thicker coating.

3.2. Tribological Properties

Figure 6 presents the friction coefficient of both the TC4 alloy and the composite MAO coatings with different concentrations of Si_3N_4/TaC particles against the GCr15 steel ball in the artificial seawater, which showed that the friction coefficient of the TC4 alloy fluctuated significantly and reached about 0.5 after nearly 5 min. The friction coefficients of the MAO coatings with different concentrations of Si_3N_4/TaC particles all first increased due to the high initial surface roughness and then decreased due to the improvement of the surface contact condition between the protrusions and the GCr15 steel ball with the sliding time [27,30]. For the high hardness of the MAO coatings, their friction coefficients were lower and experienced less fluctuation compared to the TC4 alloy. It was also observed from Figure 6 that the MAO coatings, without the addition of the Si_3N_4/TaC particles, had the lowest friction coefficient of about 0.15, and the friction coefficient of the composite MAO coatings slightly increased with the concentration of Si_3N_4/TaC particles. Previous research [34] revealed that Si_3N_4 addition could improve the wear resistance of the MAO coatings and significantly reduce the friction coefficient, which was attributed to Si_3N_4 having excellent lubrication. Thus, the friction coefficient of the composite MAO coatings was a little higher than that of the MAO coatings in the absence of Si_3N_4/TaC particles, which may be associated with the addition of hard TaC particles. In order to reveal wear damages to the coatings, SEM was used to examine the worn surfaces. The morphologies of their worn surfaces are illustrated in Figure 7, showing that the TC4 alloy had the widest wear scar of 787.8 μm with a lot of furrows along the wear direction. This was ascribed to the fact that the TC4 alloy has a much lower hardness than the MAO coatings [42,43]. The wear width of the MAO coatings ranged from 358.2 to 445.3 μm, which is significantly lower than the wear width of the TC4 alloy. This indicated that the MAO coatings greatly improved the tribological properties of the TC4 alloy, regardless of the addition of Si_3N_4/TaC particles.

The wear width of the composite MAO coatings was lower than that of the particle-free coatings and slightly increased with the concentration of Si_3N_4/TaC particles.

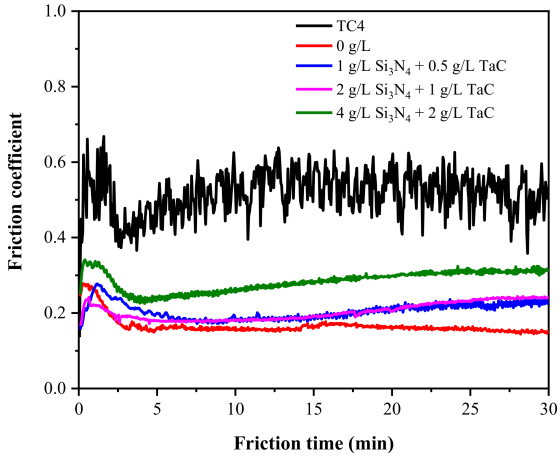

Figure 6. Friction coefficient of both the TC4 alloy and the composite MAO coatings with different concentration of Si_3N_4/TaC particles.

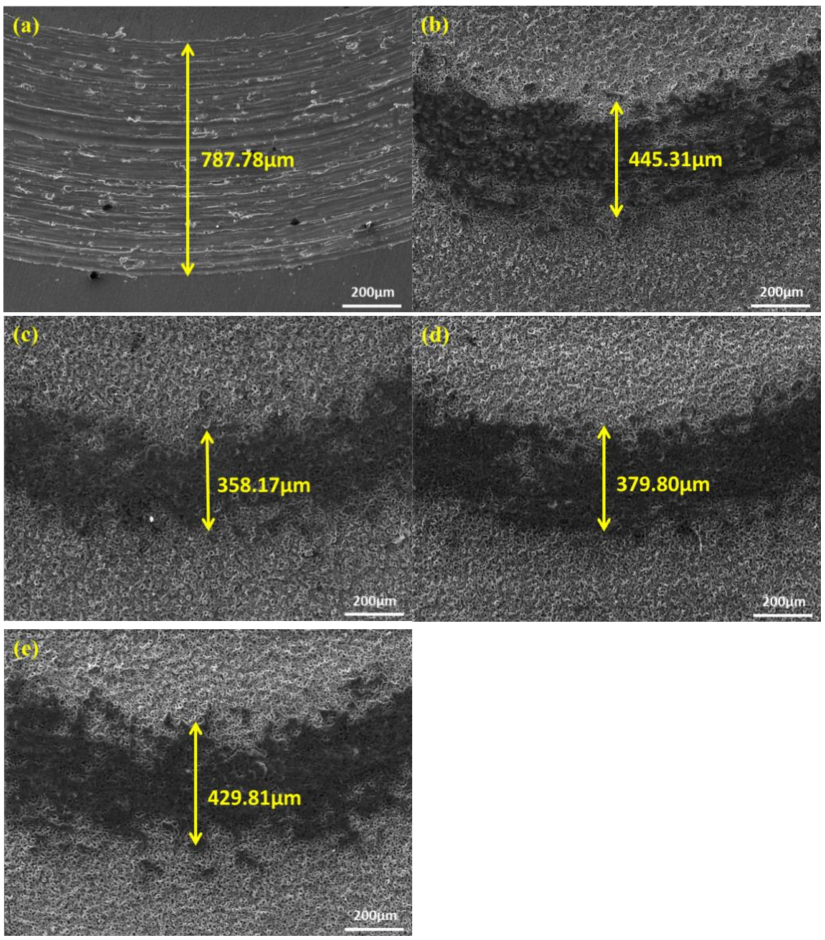

Figure 7. SEM image of the wear scar of both the TC4 alloy and the composite MAO coatings with different concentration of Si3N4/TaC particles: (**a**) TC4; (**b**) 0 g/L; (**c**) 1 g/L Si_3N_4 + 0.5 g/L TaC; (**d**) 2 g/L Si_3N_4 + 1 g/L TaC; (**e**) 4 g/L Si_3N_4 + 2 g/L TaC.

3.3. Corrosion Resistance

The potentiodynamic polarization curves of the TC4 alloy and the composite MAO coatings with the different concentrations of Si_3N_4/TaC particles in the artificial seawater were plotted in Figures 8 and 9, respectively. The relevant electrochemical data are listed in Table 5. It could be easily found from Figures 8 and 9 and Table 5 that the addition of Si_3N_4/TaC particles caused the corrosion potential (E_{corr}) of the composite coatings to move to a positive direction and the current densities decrease by about three orders of magnitude, indicating that the corrosion resistance of the composite coatings was significantly improved compared with the TC4 alloy substrate. Moreover, as can be seen from Figures 8 and 9 and Table 5, the corrosion potential of the particle-free MAO coatings reached −0.176 V_{SCE}, which was significantly higher than that of the TC4 alloy substrate, with a minimum corrosion potential of −1.229 $V_{SCE.}$ The corrosion current densities (I_{corr}) of the particle-free coatings were a little bit higher than that of the TC4 alloy substrate, which was attributed to the fact that the particle-free coatings have high porosity (19.5%) (Figure 4). In general, the corrosion resistance of the MAO coatings mainly depends on the porosity, thickness, and composition of the coating. Chen et al. [29] investigated the corrosion resistance of the MoS_2-modified MAO coatings on the titanium alloy with different MoS_2 concentrations of 0, 2, 4, 6, and 8 g/L in a 3.5 wt. % NaCl solution and the results showed that the addition of MoS_2 could significantly improve the corrosion resistance of the MAO coating and that the MoS_2-modified MAO coating with an additional amount of 4 g/L possessed the minimum porosity and average pore size and hence showed the best corrosion resistance. Therefore, it was easily understood that for the minimum porosity of 11.5%, the composite MAO coatings incorporated with the concentration of 1 g/L Si_3N_4 + 0.5 g/L TaC particles had the optimal corrosion properties in the artificial seawater.

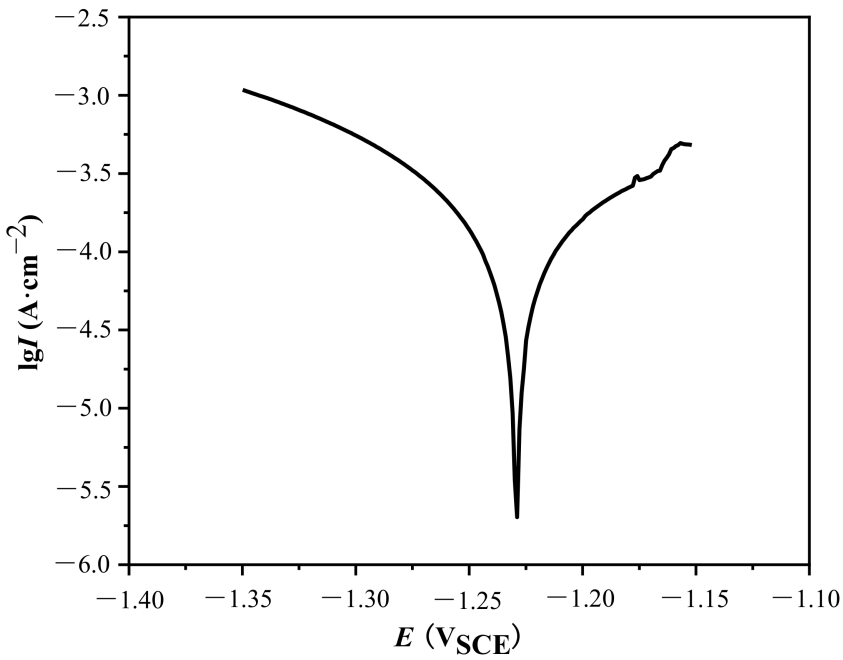

Figure 8. Potentiodynamic polarization curves of TC4 alloy in the artificial seawater.

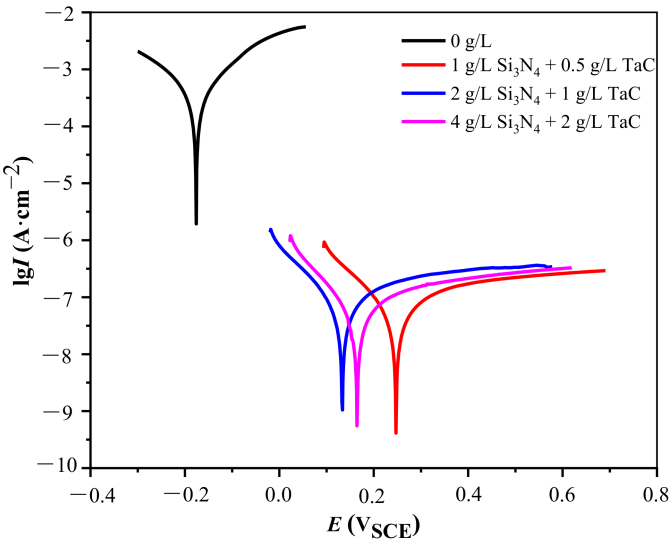

Figure 9. Potentiodynamic polarization curves of the MAO coatings with different concentration of Si_3N_4/TaC particles in the artificial seawater.

Table 5. Potentials and current densities of both the TC4 alloy and the composite MAO coatings with different concentration of Si_3N_4/TaC particles.

Specimen	TC4	0 g/L	1 g/L + 0.5 g/L	2 g/L + 1 g/L	4 g/L + 2 g/L
E_{corr}, V_{SCE}	−1.229	−0.176	0.246	0.135	0.165
I_{corr}, $A{\cdot}cm^{-2}$	8.47×10^{-5}	2.67×10^{-4}	4.23×10^{-8}	6.43×10^{-8}	4.15×10^{-8}

4. Discussions

Figure 6 shows that the TC4 alloy suffered excessive abrasive wear and that the MAO coatings with different concentrations of Si_3N_4/TaC particles were slightly worn during the friction test. To investigate the effect of the Si_3N_4/TaC particles on the tribological behaviors of both the TC4 alloy and the composite MAO coatings with different concentrations of Si_3N_4/TaC particles against the GCr15 steel ball in the artificial seawater, EDS mapping was used to reveal the distribution of the Si_3N_4/TaC particles in the wear scars (Figure 10). The EDS results showed that only 0.1 wt. % Fe was distributed in the wear scar of the TC4 alloy, whereas 2–3 wt. % Fe existed in the wear scar of the composite MAO coatings (Table 6), which indicated that the composite coatings had an excellent anti-wear effect. In addition, only about 0.3 wt. % V and 1.6 wt. % Al was detected in the wear scar of the composite MAO coatings, revealing that the coatings were not destroyed during the friction test. The low hardness TC4 alloy substrate was directly exposed to the artificial seawater and was easily worn by the high hardness GCr15 grinding ball; thus an abrasive wear scar, with deep and wide furrows, was observed (Figure 7a). It was well established that due to the ceramic-like characteristics with relatively thick and dense structures, the MAO coatings that possessed the characteristics with relatively thick and dense structures had excellent hardness properties and better tribological performance. Lan et al. [44] revealed that the wear failure mechanisms of the MAO coatings in the artificial seawater were abrasive wear and adhesive wear. It was well known that when a certain number of the Si_3N_4/TaC particles were embedded into the micropores of the MAO coatings by means of inert or reactive incorporation, those particles could play an important role in micro-lubrication and micro-cutting [45], which greatly reduced the friction coefficient of the composite MAO coatings. As shown in Figure 2c–e, the bright particles were distributed not only in the microholes but also on the flat surface to form the micro-bulges. During the friction process, these micro-bulges or micro-bumps became the main contact points to bear the normal and shear force against the GCr15 grinding ball. Thus, during the friction test, a lot of wear

debris was plowed by the micro bumps in the MAO coatings from the GCr15 grinding ball surface to fill into the micropores of the coatings or adhere to the surface of the coating. Meanwhile, the hard Si_3N_4 or TaC particles in the MAO coating adhered to the surface of the GCr15 grinding ball. Furthermore, the Si_3N_4/TaC particles dispersed throughout the composite MAO coatings, thus improving the strength of the MAO coating and further reducing the width of the wear scar during the friction process. This was evident by the fact that the MAO coating with Si_3N_4/TaC particles showed a narrower wear scar compared to the MAO coating without Si_3N_4/TaC particles (Figure 7). Particularly, the composite MAO coating fabricated with the addition of 1 g/L Si_3N_4 + 0.5 g/L TaC particles possessed a uniform distribution of Si_3N_4/TaC particles (Figure 10c), showing the narrowest wear scar (Figure 7), thus appearing to have the best tribological properties.

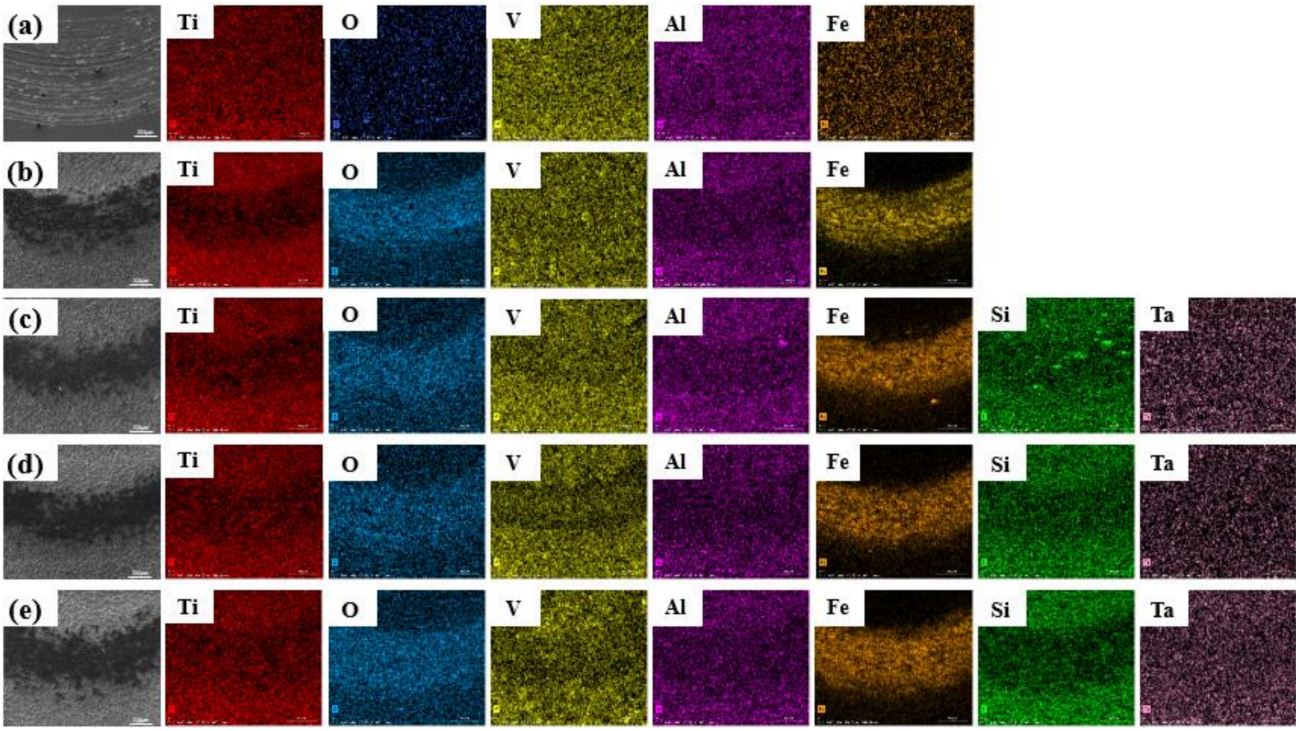

Figure 10. EDS mapping of the wear scar of both the TC4 alloy and the composite MAO coatings with different concentration of Si_3N_4/TaC particles: (**a**) TC4; (**b**) 0 g/L; (**c**) 1 g/L Si_3N_4 + 0.5 g/L TaC; (**d**) 2 g/L Si_3N_4 + 1 g/L TaC; (**e**) 4 g/L Si_3N_4 + 2 g/L TaC.

Table 6. Percentage of elements of the wear scar of both the TC4 alloy and the composite MAO coatings with different concentration of Si_3N_4/TaC particles (wt. %).

Specimen	O	Ti	V	Al	Si	Ta	Fe
TC4	19.4	71.7	3.1	6.3	-	-	0.1
0 g/L	72.3	17.7	0.3	1.6	-	-	3.0
1 g/L + 0.5 g/L	72.5	16.6	0.3	1.6	2.7	0.2	2.1
2 g/L + 1 g/L	71.8	15.0	0.3	1.6	4.5	0.5	2.3
4 g/L + 2 g/L	71.5	12.4	0.3	1.5	8.9	0.7	2.4

The corrosion properties of the MAO coatings mainly depended on the porosity, composition, and thickness of the coatings [16,44]. When the artificial seawater solution was used as the electrolyte, the MAO coating substrate and the inside of the microholes acted as the cathode and the anode, respectively. Galvanic corrosion could occur in the inside of the microholes as the anode coupled with the coating substrate caused the microholes to penetrate through the coatings and thus finally caused the corrosion of the TC4 alloy.

Figure 11 schematically shows the corrosion resistance mechanism of the MAO coatings with the different concentrations of the effect of the Si_3N_4/TaC particles. It was well reported that the coating defects, e.g., the surface porosity, deep cracks, and coating thickness, could affect the corrosion resistance of the MAO coatings [25,46–48]. As seen in Figure 3 and Table 2, the addition of Si_3N_4/TaC particles not only increases the coating thickness of the MAO coatings but also reduces the surface porosity, size, and the number of microholes in the MAO coatings. It was easy to understand that the coatings with the thicker coating and the lower surface porosity caused the corrosion electrolyte to be difficult to penetrate into the substrate. However, the open voids and channels in the coatings provide shortcuts for the corrosive electrolyte to penetrate into the substrate, thus weakening protection for the substrate. The MAO coatings with the addition of 1 g/L Si_3N_4 + 0.5 g/L TaC particles, whose surface porosity and thickness were 11.85% and 20.6 µm, respectively, had better corrosion properties than that of the MAO coatings with the addition of 4 g/L Si_3N_4 + 2 g/L TaC particles, whose surface porosity and thickness were 12.35% and 22.0 µm, respectively, indicating that surface porosity might be a more important influence factor than the thickness on the corrosion properties of the MAO coatings.

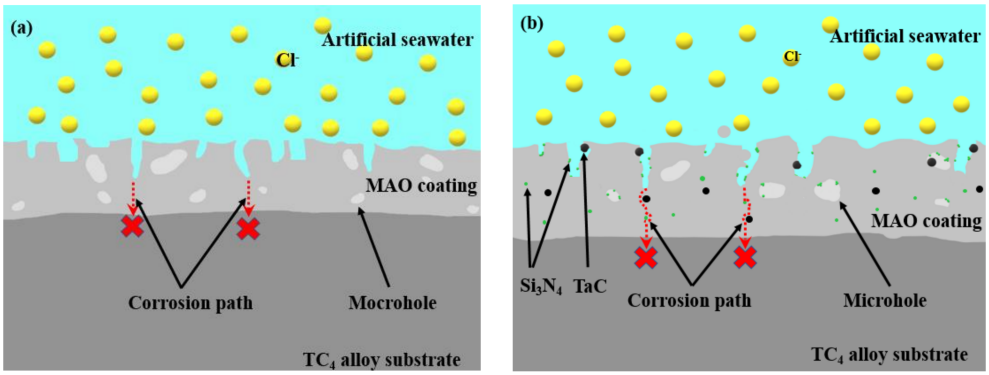

Figure 11. Corrosion resistance mechanism of the MAO coatings with and without Si_3N_4/TaC particles: (**a**) MAO coating without Si_3N_4/TaC particles; (**b**) MAO coating with Si_3N_4/TaC particles.

5. Conclusions

(1) The phase constituents of the composite MAO coatings with different contents of Si_3N_4/TaC particles were mainly composed of anatase TiO_2, rutile TiO_2, TaC, Si_3N_4, and $Al_4Ti_2SiO_{12}$. By increasing the concentration of the Si_3N_4/TaC particles, the peak intensity of rutile TiO_2 and TaC gradually increased, and the content of the metastable anatase-TiO_2 decreased.

(2) For the inert or partly-reactive incorporation of Si_3N_4/TaC particles during the MAO process, the thickness of the composite MAO coatings gradually increased with the increment of the concentration of Si_3N_4/TaC particles. The porosity of the MAO coatings first decreased and then increased with the increasing concentration of Si_3N_4/TaC particles.

(3) The MAO coatings greatly improved the tribological properties of the TC4 alloy in the artificial seawater solution, regardless of the addition of the Si_3N_4/TaC particles. The composite MAO coatings with 1 g/L Si_3N_4 + 0.5 g/L TaC particles presented a relatively lower friction coefficient and the narrowest wear scar, thus showing the best tribological properties.

(4) The addition of Si_3N_4/TaC particles could enhance the corrosion resistance of the MAO coatings. The composite MAO coatings with 1 g/L Si_3N_4 + 0.5 g/L TaC particles exhibited the highest corrosion potential and the lower current density, i.e., the optimal corrosion resistance in the artificial seawater solution. This could be attributed to the fact that the coating had the lowest surface porosity.

Author Contributions: Conceptualization, W.Y. and J.L.; methodology, W.G.; software, L.W.; validation, Y.J., Y.Y. and L.W.; formal analysis, W.G. and Z.D.; investigation, W.Y.; resources, J.L.; data curation, Z.D.; writing—original draft preparation, W.G. and Z.D.; writing—review and editing, Y.J. and Y.Y.; visualization, Y.J. and Z.D.; supervision, Y.Y.; project administration, W.Y. All authors have read and agreed to the published version of the manuscript.

Funding: This research was funded by the National Natural Science Foundation of China (52071252), Key Research and Development Program of Shaanxi Province (2021ZDLSF03-11, 2021GY-208, 2022GY-407).

Institutional Review Board Statement: Not applicable.

Informed Consent Statement: Not applicable.

Data Availability Statement: Not applicable.

Conflicts of Interest: The authors declare no conflict of interest.

References

1. Jha, A.K.; Singh, S.K.; Kiranmayee, M.S.; Sreekumar, K.; Sinha, P.P. Failure analysis of titanium alloy (Ti6Al4V) fastener used in aerospace application. *Eng. Fail. Anal.* **2010**, *17*, 1457–1465. [CrossRef]
2. Ding, R.; Guo, Z.X.; Wilson, A. Microstructural evolution of a Ti–6Al–4V alloy during thermomechanical processing. *Mater. Sci. Eng. A* **2002**, *327*, 233–245. [CrossRef]
3. Rack, H.J.; Qazi, J.I. Titanium alloys for biomedical applications. *Mater. Sci. Eng. C* **2006**, *26*, 1269–1277. [CrossRef]
4. Yang, W.; Gao, Y.; Guo, P.; Xu, D.P.; Wang, A.Y. Adhesion, biological corrosion resistance and biotribological properties of carbon films deposited on MAO coated Ti substrates. *J. Mech. Behav. Biomed.* **2020**, *101*, 103448. [CrossRef] [PubMed]
5. Xie, R.; Lin, N.; Peng, Z.; Zou, J.; Han, P.; Wang, Z.; Tang, B. Surface damage mitigation of TC4 alloy via micro arc oxidation for oil and gas exploitation application: Characterizations of microstructure and evaluations on surface performance. *Appl. Surf. Sci.* **2018**, *436*, 467–476. [CrossRef]
6. Mousavi-Semnani, S.Z.; Yousefpour, M.; Zareidoost, A. Enhancing the biocompatibility of ZrO_2 thin film on Zr–2.5Nb alloy by anodizing treatment using an electrolyte containing biofunctional groups. *Thin Solid Films* **2022**, *753*, 139279. [CrossRef]
7. Deng, H.Y.; Xu, K.X.; Liu, S.G.; Zhang, C.F.; Zhu, X.W.; Zhou, H.R.; Xia, C.Q.; Shi, C.B. Impact of engineering surface treatment on surface properties of biomedical TC4 Alloys under an artificial human environment. *Coatings* **2022**, *12*, 157. [CrossRef]
8. Huang, J.; Ma, J.; Wu, L.; Wei, J.; Li, H. Microstructure and wear resistance of WS_2/W composite coating on TC4 titanium alloy surface. *J. Phys. Conf. Ser.* **2021**, *1885*, 032046. [CrossRef]
9. Salman, S.H.; Shihab, A.A.; Kh.Elttayef, A.H. Design and construction of nanostructure TiO_2 thin film gas sensor prepared by R.F magnetron sputtering technique. *Energy Procedia* **2019**, *157*, 283–289. [CrossRef]
10. Wu, S.K.; Yang, W.; Gao, W.; Yao, Y.H.; Zhang, Y.; Chen, J. Characterization of MAO + Cu composite coatings on aluminum alloy. *Coatings* **2021**, *11*, 1172. [CrossRef]
11. Da Silva Rodrigues, J.; Antonini, L.M.; da Cunha Bastos, A.A.; Zhou, J.; de Fraga Malfatti, C. Corrosion resistance and tribological behavior of ZK30 magnesium alloy coated by plasma electrolytic oxidation. *Surf. Coat. Technol.* **2021**, *410*, 126983. [CrossRef]
12. Gao, J.; Zheng, K.; Yu, S.W.; Hei, H.J.; Wu, Y.X.; Gong, H.R.; Ma, Y. Characterization of quasi-static/dynamic contact mechanical properties of Mo surface-modified TC4. *Coatings* **2002**, *12*, 123. [CrossRef]
13. Chen, C.A.; Jian, S.Y.; Lu, C.H.; Lee, C.Y.; Aktuğ, S.L.; Ger, M.D. Evaluation of microstructural effects on corrosion behavior of AZ31B magnesium alloy with a MAO coating and electroless Ni–P plating. *J. Mater. Res. Technol.* **2020**, *9*, 13902–13913. [CrossRef]
14. Asl, V.Z.; Chini, S.F.; Zhao, J.; Palizdar, Y.; Shaker, M.; Sadeghi, A. Corrosion properties and surface free energy of the ZnAl LDH/rGO coating on MAO pretreated AZ31 magnesium alloy. *Surf. Coat. Technol.* **2021**, *426*, 127764.
15. Song, Y.; Wang, H.; Liu, Q.; Li, G.; Wang, S.; Zhu, X. Sodium dodecyl sulfate (SDS) intercalated MgAl layered double hydroxides film to enhance the corrosion resistance of AZ31 magnesium alloy. *Surf. Coat. Technol.* **2021**, *422*, 127524. [CrossRef]
16. Wang, Y.M.; Jiang, B.L.; Lei, T.Q.; Guo, L.X. Dependence of growth features of microarc oxidation coatings of titanium alloy on control modes of alternate pulse. *Mater. Lett.* **2004**, *58*, 1907–1911. [CrossRef]
17. Wang, Y.M.; Jia, D.C.; Guo, L.X.; Lei, T.Q.; Liang, B.L. Effect of discharge pulsating on microarc oxidation coatings formed on Ti6Al4V alloy. *Mater. Chem. Phys.* **2005**, *90*, 128–133. [CrossRef]
18. Xue, W.B.; Wang, C.; Deng, Z.W.; Chen, R.Y.; Zhang, T.H. Influence of electrolytes on the microstructure of microarc oxidation coatings on Ti–6Al–4V alloy. *J. Mater. Sci. Technol.* **2002**, *18*, 37–39.
19. Yang, W.; Xu, D.P.; Guo, Q.Q.; Chen, T.; Chen, J. Influence of electrolyte composition on microstructure and properties of coatings formed on pure Ti substrate by micro arc oxidation. *Surf. Coat. Technol.* **2018**, *349*, 522–528. [CrossRef]
20. Yao, Z.P.; Xu, Y.J.; Jiang, Z.H.; Wang, F.P. Effects of cathode pulse at low frequency on the structure and composition of plasma electrolytic oxidation ceramic coatings. *J. Alloys Compd.* **2009**, *488*, 273–278. [CrossRef]
21. Gao, W.; Liu, J.N.; Wei, J.P.; Yao, Y.H.; Ma, X.Q.; Yang, W. Enhanced properties of micro arc oxidation coating with Cu addition on TC4 alloy in marine environment. *Coatings* **2021**, *11*, 1168. [CrossRef]

22. Zhang, Y.; Yang, W.; Yu, S.; Wang, L.Q.; Ma, X.Q.; Gao, W.; Lan, N.; Shao, W.T. Microstructure and properties in artificial seawater of copper-doped micro-arc coatings on TC4 alloy. *Coatings* **2022**, *12*, 883. [CrossRef]
23. Rafieerad, A.R.; Ashra, M.R.; Mahmoodian, R.; Bushroa, A.R. Surface characterization and corrosion behavior of calcium phosphate-base composite layer on titanium and its alloys via plasma electrolytic oxidation: A review paper. *Mater. Sci. Eng. C* **2015**, *57*, 307–413. [CrossRef] [PubMed]
24. Muhaffffel, F.; Kaba, M.; Cempura, G.; Derin, B.; Kruk, A.; Atar, E.; Cimenoglu, H. Influence of alumina and zirconia incorporations on the structure and wear resistance of titania-based MAO coatings. *Surf. Coat. Technol.* **2019**, *377*, 124900. [CrossRef]
25. Lu, X.P.; Mohedano, M.; Blawert, C.; Matykina, E.; Arrabal, R.; Kainer, K.U.; Zheludkevich, M.L. Plasma electrolytic oxidation coatings with particle additions—A review. *Surf. Coat. Technol.* **2016**, *307*, 1165–1182. [CrossRef]
26. Wang, C.; Hao, J.M.; Xin, Y.Z.; Guo, C.F.; Chen, H. High temperature oxidation behavior of TiO_2 + ZrO_2 composite ceramic coatings prepared by microarc oxidation on Ti6Al4V alloy. *Surf. Coat. Technol.* **2015**, *215*, 201–207. [CrossRef]
27. Wang, S.X.; Zhao, Q.; Liu, D.X.; Du, N. Microstructure and elevated temperature tribological behavior of TiO_2/Al_2O_3 composite ceramic coating formed by microarc oxidation of Ti6Al4V alloy. *Surf. Coat. Technol.* **2015**, *272*, 343–349. [CrossRef]
28. Mu, M.; Liang, J.; Zhou, X.; Xiao, Q. One-step preparation of TiO_2/MoS_2 composite coating on Ti6Al4V alloy by plasma electrolytic oxidation and its tribological properties. *Surf. Coat. Technol.* **2013**, *214*, 124–130. [CrossRef]
29. Chen, X.W.; Li, M.L.; Zhang, D.F.; Cai, L.P.; Ren, P.; Hu, J.; Liao, D.D. Corrosion resistance of MoS_2-modified titanium alloy micro-arc oxidation coating. *Surf. Coat. Technol.* **2022**, *433*, 128127. [CrossRef]
30. Ao, N.; Liu, D.X.; Wang, S.X.; Zhao, Q.; Zhang, X.H.; Zhang, M.M. Microstructure and tribological behavior of a TiO_2/hBN composite ceramic coating formed via micro-arc oxidation of Ti–6Al–4V alloy. *J. Mater. Sci. Technol.* **2016**, *32*, 1071–1076. [CrossRef]
31. Lou, B.S.; Lin, Y.Y.; Tseng, C.M.; Lu, Y.C.; Duh, J.G.; Lee, J.W. Plasma electrolytic oxidation coatings on AZ31 magnesium alloys with Si_3N_4 nanoparticle additives. *Surf. Coat. Technol.* **2017**, *332*, 358–367. [CrossRef]
32. Lu, X.P.; Blawert, C.; Scharnagl, N.; Kainer, K.N. Influence of incorporating Si_3N_4 particles into the oxide layer produced by plasma electrolytic oxidation on AM50 Mg alloy on coating morphology and corrosion properties. *J. Magnes. Alloy* **2013**, *1*, 267–274. [CrossRef]
33. Aliofkhazraei, M.; Sabour Rouhaghdam, A.; Shahrabi, T. Abrasive wear behavior of Si_3N_4/TiO_2 nanocomposite coatings fabricated by plasma electrolytic oxidation. *Surf. Coat. Technol.* **2010**, *205*, S41–S46. [CrossRef]
34. Gao, W.; Liu, J.N.; Ding, Z.S.; Zhang, Y.; Yao, Y.H.; Yang, W. Influence of Si_3N_4 nanoparticles on microstructure and properties of microarc oxidation coatings on TC4 alloy. *Rare Metal Mater. Eng.* **2022**, *51*, 1537–1542.
35. Zhang, X.H.; Hilmas, G.E.; Fahrenholtz, W.G. Densification and mechanical properties of TaC-based ceramics. *Mater. Sci. Eng. C* **2009**, *501*, 37–43. [CrossRef]
36. Ding, Z.S.; Gao, W.; Wei, J.P.; Jin, Y.H.; Zhao, C.; Yang, W. Effects of TaC microparticles on structure and properties of micro-arc oxidation coating on Ti–6Al–4V alloy. *Acta Phys. Sin.* **2022**, *71*, 028102. [CrossRef]
37. Wang, F.; Wang, X.H.; Xie, W.E.; Wang, F.; Gan, Q.; Ping, S.; Wei, J.; Li, F.Q.; Wang, Z.M. Simultaneous incorporation of gallium oxide and tantalum microparticles into micro-arc oxidation coating of titanium possessing antibacterial effect and stimulating cellular response. *Biomater. Adv.* **2022**, *135*, 212736. [CrossRef]
38. Zhang, S.L.; Zou, X.R.; Liu, N.; Wang, H.R.; Xia, C.Q.; Liang, C.Y. In situ preparation of a novel Ta_2O_5/MAO composite coating on magnesium for anti-corrosion protection. *Surf. Coat. Technol.* **2022**, *430*, 128003. [CrossRef]
39. Du, N.; Wang, S.X.; Zhao, Q.; Zhu, W.H. Microstructure and tribological properties of microarc oxidation composite coating containing Cr_2O_3 particles on TC4 titanium alloy. *Rare Metal Mater. Eng.* **2013**, *42*, 621–624.
40. Gleiter, H. Nanostructured materials: Basic concepts and microstructure. *Acta Mater.* **2000**, *48*, 1–29. [CrossRef]
41. Qi, W.H.; Wang, M.P. Size and shape dependent melting temperature of metallic nanoparticles. *Mater. Chem. Phys.* **2004**, *88*, 280–284. [CrossRef]
42. Xue, W.B.; Wang, C.; Chen, R.Y.; Deng, Z.W. Structure and properties characterization of ceramic coatings produced on Ti–6Al–4V alloy by microarc oxidation in aluminate solution. *Mater. Lett.* **2002**, *52*, 435–441. [CrossRef]
43. Wang, Y.M.; Jiang, B.L.; Lei, T.Q.; Guo, L.X. Microarc oxidation coatings formed on Ti6Al4V in Na_2SiO_3 system solution: Microstructure, mechanical and tribological properties. *Surf. Coat. Technol.* **2006**, *201*, 82–89. [CrossRef]
44. Lan, N.; Yang, W.; Gao, W.; Guo, P.; Zhao, C.; Chen, J. Characteristic of ta–C film on micro arc oxidation coated titanium all in artificial seawater. *Diam. Relat. Mater.* **2021**, *117*, 108483. [CrossRef]
45. Jin, F.Y.; Chu, P.K.; Tong, H.H.; Zhao, J. Improvement of surface porosity and properties of alumina films by incorporation of Fe micrograins in micro-arc oxidation. *Appl. Surf. Sci.* **2006**, *253*, 863–868. [CrossRef]
46. Muhaffel, F.; Cimenoglu, H. Development of corrosion and wear resistant micro-arc oxidation coating on a magnesium alloy. *Surf. Coat. Technol.* **2019**, *357*, 822–832. [CrossRef]
47. Lou, B.S.; Lee, J.W.; Tseng, C.M.; Lin, Y.Y.; Yen, C.A. Mechanical property and corrosion resistance evaluation of AZ31 magnesium alloys by plasma electrolytic oxidation treatment: Effect of MoS_2 particle addition. *Surf. Coat. Technol.* **2018**, *350*, 813–822. [CrossRef]
48. Laleh, M.; Rouhaghdam, A.S.; Shahrabi, T.; Shanghi, A. Effect of alumina sol addition to micro-arc oxidation electrolyte on the properties of MAO coatings formed on magnesium alloy AZ91D. *J. Alloys Compd.* **2010**, *496*, 548–552. [CrossRef]